TENSILE BEHAVIOUR OF A NANOCRYSTALLINE BAINITIC STEEL CONTAINING 3 WT% SILICON.

C. Garcia-Mateo[A], F.G. Caballero[A], T. Sourmail[B], M. Kuntz[C], J. Cornide[A], V. Smanio[B], R. Elvira[D]

[A]Department of Physical Metallurgy. National Center for Metallurgical Research (CENIM-CSIC), MATERALIA Research Group. Avda. Gregorio del Amo, 8, 28040, Madrid, Spain.

[B]Ascometal-CREAS (research centre) Metallurgy, BP 70045 57301 Hagondange Cedex, France

[C]Robert Bosch GmbH, Materials- and Process Engineering Metals, P.O. Box 30 02 40, 70442 Stuttgart, Germany.

[D] Gerdau Sidenor I+D, S.A. Barrio Ugarte, s/n, 48970 Basauri, Spain

Corresponding Author : Carlos Garcia-Mateo. cgm@cenim.csic.es. Tf: +34 91 5538900 Fax: 34 91 534 74 25. Centro Nacional de Investigaciones Metalurgicas (CENIM-CSIC). Avda. Gregorio del Amo 8. Madrid E-28040. Spain.

Abstract

Much recent work has been devoted to characterize the microstructure and mechanical properties bainitic nanostructured steels. The microstructure is developed by isothermal heat treatment at temperatures as low as 125-350ºC and adapted steel grades typically contain high carbon contents to achieve sufficient depletion of the B_S-M_S temperature range, and above 1.5 Si wt.% to suppress carbide formation during isothermal holding. On the latter, most of the published literature agrees on a limit of around 1.2-1.5 wt.% to suppress cementite in high carbon steels. For this reason perhaps, additions of Si significantly above this limit have not been investigated systematically in the context of nanostructured bainitic steels. The present work is concerned with the effect of up to ~3 Si wt.% in a steel grade otherwise adapted to low temperature bainitizing. Tensile properties as compared to similar grades, though with lower Si contents, exhibited unrivalled combinations of strength and ductility, with above 21% total elongation for a UTS above 2GPa. An attempt is made to explain the mechanical properties of this microstructure in terms of some of its most relevant and unique morphological and microstructural features.

Keywords: bainite, nanostructures ferrite, mechanical properties, TRIP

1 INTRODUCTION

Grain refinement is a well known and widely used method to achieve combinations of ductility and high strength in metallic materials. In heat-treatable material, this refinement can be achieved not only through complex thermomechanical processing but also through simple heat-treatments schedules [1]. An example of the latter is low temperature bainitizing, whereby one achieves a microstructure of bainitic ferrite plates a few tens of nanometres thick [2-4]. Indeed the degree of refinement achievable during low temperature bainitizing is such that the topic has received unprecedented attention in recent years [5-10].

It is established [11] that the bainitic ferrite plate thickness depends primarily on two factors, first the strength of the austenite at the transformation temperature and second, the chemical free energy change accompanying transformation. Thus, strong austenite or a large driving force results in finer plates, the former because there is a large resistance to interface motion and the latter because an increased nucleation rate leads to microstructural refinement. Both, austenite strength and driving force, increase as the transformation temperature decreases. In previous experiences [2-4] the design of low temperature bainitic steels was based on the decrease of the B_S-M_S temperature range by chemical composition control and the increase in the transformation driving force, to achieve adequate transformation times consistent with the requirements of industrial manufacturing, by Co and/or Al additions. However, due to the cost of raw material (Co) and the incompatibility of high Al additions with cleanliness requirements of ultra high strength steels, both alloys are unlikely to find industrial use.

It is known that Si is a strong austenite solid solution hardener [12,13], therefore inclusion of this element in much higher quantities, in principle, is a way to ensure that the bainite growth results in even finer plates. Silicon is originally added to the chemical composition of this type of nanostructured steels in quantities close to 1.5 wt.% in order to retard and to some extent to avoid cementite precipitation from austenite during bainite reaction. In this work, silicon additions are increased up to 3 wt.% to get an extra strengthening in the austenite prior to bainite reaction. According to Ref. 12, an increase of 1.5 wt.% of Si

implies an increase of 7% in the YS of austenite. Both, Co and Al, accelerate bainite transformation, therefore their absence in the chemical composition was compensated by reducing the quantities of Mn and Cr present [14]. As in the other cases, the design was based on phase transformation theory [15] and other well known metallurgical facts [16-18].

Results will be presented that demonstrate unprecedented levels of ductility at strength above 2 GPa.

2 MATERIAL AND EXPERIMENTAL PROCEDURE

The designed alloy has a chemical composition, Table 1, with enough C to ensure low transformation temperatures and 3 wt.% Si to ensure solid solution strengthening as well as to avoid cementite precipitation. As Co and Al, no longer present in the chemical composition, have an accelerating effect on bainitic transformation, Cr and Mn were kept as low as possible to maintain the transformation times with the range of the Co and Co+Al alloys, and, at the same time, to ensure sufficient hardenability to avoid transformation during cooling from the austenitisation temperature to the bainite transformation temperature. For this purposes 0.45 and 0.77 wt.% of Cr and Mn were added to the chemical composition, an important reduction if compared with 1 and 2 wt.% of Cr and Mn in the Co and Co+Al alloys [4].

The alloy was produced as a 40 kg ingots and forged to a final diameter of about 50 mm. Cuts of about 15x15x100 mm^3 (tensile tests pre-forms) were austenitised at 950ºC for 60 min, then transferred to a salt bath at the required bainitizing temperature. Bainitizing was thus carried out at 250ºC and 220ºC for 16 and 22 h respectively, to achieve a completely bainitic microstructure. Those reactions times compare well with those reported in ref.4, validating the design process in terms of obtaining similar transformation kinetics as those of the benchmark alloys but without the use of expensive alloys elements as Co and Al.

To reveal the microstructure, metallographic samples were cut, ground and polished following the standard procedures. A 2% Nital etching solution was used to reveal bainitic microstructure. Scanning electron microscopy observation was carried out on a JEOL J8M-6500 field emission gun scanning electron microscope (SEM-FEG) operating at 10 kV. Before etching, samples were polished using colloidal silica suspension. High magnification SEM-FEG micrographs were used to determine the

distribution and size of the different retained austenite morphologies and also the bainitic ferrite plate thickness *t*, by measuring the mean lineal intercept $\overline{L}_T = \pi t/2$ in a direction normal to the plate length [4,19].

TEM specimens were sliced from 3-mm-diameter rods of the heat-treated material, mechanically thinned to 0.06 mm, and then twin-jet electropolished to perforation using a mixture of 5% perchloric acid, 25% glycerol and 70% ethanol at 10 ºC at 45 V. The samples were examined on a TEM JEOL 2010 transmission electron microscope operated at 200 keV.

Quantitative X-ray diffraction analysis was used to determine the fraction of retained austenite (V_γ) and its carbon content (C_γ). For this purpose, samples were machined, ground and finally polished using colloidal silica suspension. They were then step-scanned in a SIEMENS D5000 X-ray diffractometer using unfiltered Co K_α radiation. The scanning speed (2θ) was less than 0.3º/min. The machine was operated at 40 kV and 30 mA. The volume fraction of retained austenite was calculated from the integrated intensities of (200), (220) and (311) austenite peaks, and those of (002), (112) and (022) planes of ferrite. The austenite carbon content was estimated using well-known Dyson and Holmes' equation [20], that relates austenite lattice parameter to its composition. Although this expression has been validated in several works [4,21,22], further considerations should be performed to take into account the effects of substitutional elements, and those have been extensively described in other publications [23,24].

Tensile tests were performed at room temperature in specimens of 5 mm diameter and gauge length of 14 mm at a strain rate of $0.004 s^{-1}$. All experiments were assisted by an extensometer fitted to electronic equipment that allowed the continuous tracking of load-displacement data during tests. Load and elongations measured during uniaxial tensile tests were converted to engineering and true stress-strain curves. Strain hardening was characterized by the incremental strain-hardening exponent defined as $n = d(\ln\sigma)/d(\ln\varepsilon_p)$, where $\sigma = k\,\varepsilon_p^n$ represents the flow curve in the region of uniform true plastic strain and k

is the strength coefficient. Hardness was measured as HV_{10} and the presented results correspond to an average of at least 3 values.

3 RESULTS AND DISCUSSION

3.1 MICROSTRUCTURE

The microstructure consists of a mixture of two phases, bainitic ferrite and carbon enriched regions of austenite. Figure 1 (a) and (b) show optical micrographs of the microstructure obtained after heat treatment at 220 and 250ºC respectively. The lighter phases are micro-blocks of retained austenite (> 1000 nm), whereas the darker feather-like features are sheaves of bainite, groups of bainitic ferrite plates sharing a common crystallographic orientation and separated by thin films of retained austenite. Only at much higher magnification, Figure 1 (c) and (d), it is possible to observe the bainitic ferrite plates (lower relief) and the retained austenite (higher relief) as sub-micron blocks (100-1000 nm) and nano-films (< 100nm). Plastic relaxation of the shape change occurring as a consequence of the displacive growth of bainite takes places via generation of both, dislocations in the austenite/bainitic ferrite interface, as those shown in Figure 2, where extensive dislocation debris is evident in a sub-micron block of retained austenite, and also via micro/nano twins in the austenite in contact with bainitic ferrite plates [25-27].

Summary on the detailed characterization of the microstructures is presented in Table 2. In both cases, 220 and 250ºC, bainitic ferrite is the main phase, and its presence represents almost 65%. The main difference detected is in the level of austenite carbon enrichment, which is higher at 250ºC than at 220ºC. This appears at first in contradiction with the theory of bainite formation, whereby the retained austenite content is simply estimated by the lever rule as applied between ferrite and austenite of carbon content given by the T_0 line [15]. However, while this theory has been demonstrated to hold at sufficiently high temperature [16,18,28], there is increasing evidence that at least part of the carbon remains trapped in ferrite and/or dislocations when transforming at lower temperatures [22,29-32]. Thus, it may be the case the higher carbon content of the austenite after transformation at 250ºC is a consequence of the lesser trapping at this temperature when compared to 220ºC.

Table 2 confirms that bainitic ferrite plate is within the nano-range, 28 nm thick for both transformation temperatures, there is no further refinement in the microstructure when the transformation temperature is lowered from 250 to 220 ºC but a narrower distribution of plate thickness, as Figure 3 illustrates. These results come to support and validate the alloy design procedure where bainitic ferrite plate thickness was meant to keep at nano scale by acting directly on the strength of the parent austenite where it grows, instead on increasing the free energy change for transformation as in the case of the Co and Co+Al alloys in ref. 4. An extra refinement of the bainitic ferrite plates was achieved in this new alloy when compared with the benchmark alloys, i.e. 28 and 49/41 nm for the new and the Co/Co+Al alloys respectively after isothermal heat treatment at 250ºC [4].

The refinement of the microstructure to the nano scale is not exclusive of the bainitic ferrite, retained austenite trapped between the slender plates of ferrite, nano-films, as those shown in Figure 1 (c,d), have an average size of ~35 nm for both heat treatments and exhibit very similar size distribution, Figure 4. In the past, the term block of austenite has been used to describe pools of austenite with sizes of several tens of microns trapped between sheaves of bainite, and observable under light optical microscopy. In low-temperature bainitic alloys when using the term block is to denote sub-micron features of this phase, only visible under SEM, as Figure 1 (c,d) and Figure 4 show. Where it is clear that an increase in the isothermal temperature leads to both, coarser blocks of austenite, from 630 to 870 nm at 220 and 250ºC respectively, and wider distribution towards the bigger sizes.

3.2 MECHANICAL BEHAVIOUR

Figure 5 a and c shows the typical strain-stress curves from tensile tests at room temperature, of the 220 and 250ºC microstructures, the presence of mobile dislocations introduced during transformation, leads to the observed continuous yielding. Table 3 gathers the results obtained from the room temperature tensile experiments, showing an extraordinary combination of tensile properties, with yield strengths of about 1.7

GPa and ultimate tensile strengths ranging from 2 to 2.3 GPa. There are several operative strengthening mechanisms (YS) which are expected to contribute to the microstructure strength; (a) size of the bainitic ferrite plates, the thinner they are the shorter the mean free path for dislocation glide is, leading to the enhancement of the strength, (b) carbon content and (c) dislocation density in ferrite. Given that the ferrite plate thickness is the same for both conditions, and it represents the biggest contribution [33], it is not strange that the YS is so similar for both conditions. Differences in the UTS of both microstructures could be explained in terms of their work hardening capacity, Figure 5 b and d. As it will shown later, in the 250ºC microstructure at first there is a pronounced decrease of the strain-hardening that later increases, while for the 220ºC the increase of the strain-hardening is continuous and reaches higher values, explaining its higher UTS.

Ductility of nanostructured bainite.

Ductility, measured as elongation, uniform and fracture, clearly decreases as strength increases, Table 3. The microstructure obtained by transformation at 250ºC exhibits uniform and fracture elongation of 11.6 and 21.3% respectively, very high values when compared with those obtained by transformation at 220ºC, where the elongation is reduced to 7.4%, in this case all the elongation is uniform and hardly any necking was observed in the tested samples. This behaviour is also visible in the incremental strain-hardening curves, Figure 5 b and d, as anticipated, in the 220ºC there is a continuous increase towards the instability criteria, straight line in Figure 5 b and d, which is never reached, explaining the fact that all the elongation is uniform. In the case of the 250ºC microstructure, the exhibited behaviour is remarkable, i.e. after the initial rapid increase there is a decrease up to 2.5% true plastic strain, then there is a clear increase in the hardening that leads to very high values of uniform elongation (11.6%) and even higher fracture elongation (21.3%).

Stacking Fault Energy of austenite in nanostructured bainite.

Seeing the behaviour of the incremental work hardening of the 250ºC microstructure, Figure 5d**,** and the relatively high fraction of retained austenite, 35%**,** a natural question that arises, giving the similarities [34], is the possibility of TWIP (Twining Induced Plasticity) effect assisting ductility.

According to the latest literature review, [35-38], an enhancement of ductility could be attained by means of TWIP effect. The deformation mechanisms and mechanical properties of face-centered cubic (fcc) metals, as austenite, are strongly related to their stacking fault energy (SFE) γ^* [35], which is the most crucial nucleation parameter determining whether twinning, martensite transformation or dislocation glide alone will occur during deformation of the material. SFE is defined as $\gamma^* = 2\rho\Delta G^{\gamma\to\varepsilon} + 2\sigma$, where $\Delta G^{\gamma\to\varepsilon}$ is the molar Gibbs energy of the transformation, $\rho = 4/(a^2 N\sqrt{3})$ is the molar surface density, a is the lattice parameter and N the Avogadro number, and σ is the surface energy of the interface γ/ε,with a value between 8-9 mJ m^{-2}. TWIP effect is said to occur when SFE lies in the range 12-18 mJ $m^{-2} < \gamma^* <$ 35-45 mJ m^{-2}.

The necessary thermodynamic calculations have been performed by means of MTDATA [39]. To calculate the free energy change for γ to ε transformation, $\Delta G^{\gamma\to\varepsilon}$, the chemical composition of the retained austenite present at both conditions, 220 and 250ºC, and derived from X-ray experiments, Table 2, were used. The lattice parameter necessary for the SFE calculation is listed in Table 2.

To make sure of the consistence of the calculation procedure, the SFE was also calculated for a typical TWIP steel (0.08C, 27Mn, 0.52 Si, 4.1 Al) from ref. [35], and the results thus obtained were compared with those reported in the same publication, finding that both were almost identical, see Table 4. The SFE values reported for retained austenite of the 220 and 250ºC microstructures are one order of magnitude bigger than those of the TWIP steel, and completely out of the range where TWIP is expected to take place. Therefore, and according to the calculations, no TWIP effect should be expected in the studied conditions.

Therefore, once that the possibility of TWIP effect assisting ductility is ruled out, an attempt to explain the very distinctive ductility behaviours is made in the following paragraphs, based on the microstructural peculiarities of both heat treatments.

Rationalizing ductility and TRIP effect of nanostructured bainite.

It is believed that in bainitic steels ductility is mainly controlled by the amount of retained austenite [40], which is a ductile phase when compared with bainitic ferrite (hard phase), and it would be expected to enhance ductility as far as austenite is homogeneously distributed between plate boundaries (film austenite), contributing to suppress crack and/or void initiation at the grain boundary. However, isolated pools of austenite (blocky austenite) would influence unfavorably on both elongation and strength presumably, because of the strain localization in these areas [41]. Further improvement in ductility can be achieved by TRIP effect i.e. strain induced transformation of retained austenite to martensite. The transformation implies a relaxation of the local stress concentration and extra strain hardening by means of two sources; (a) progressive increase in volume fraction of a hard phase and (b) additional plastic deformation due to transformation strains. In order to take full advantage of this effect, the mechanical stability of austenite, i.e. its capability to transform to martensite under strain, must be moderate. Morphology is an important factor to be considered on the mechanical stability of austenite. In terms of its mechanical stability, thin films of retained austenite can be too stable [42,43] to transform by TRIP effect, and several are the reasons. First, because of the constraint to transformation exerted by the surrounding plates of ferrite, second, because smaller retained austenite contain lower potential nucleation sites for the transformation to martensite therefore requiring higher driving force for martensite nucleation. And finally, because their higher carbon concentration [25]. In this sense, the chemical composition is an important factor controlling the mechanical stability of austenite. Elements such as C, Mn and Si [44,45] significantly enhance the austenite mechanical stability, among them C is the element that exhibits the strongest influence. In alloys containing austenite of low mechanical stability, the strain-induced transformation occurs in early stages of deformation, resulting in little or null benefit of the strain hardening related to deterring plastic instability or necking in the later stages of deformation. On the other hand, if austenite becomes mechanically more stable and transforms at higher strains, hence the associated strain hardening effectively increases resistance to necking and fracture. However, if austenite is too stable, the presence of large amounts of austenite at necking (instability criterion) does not guarantee effective TRIP effect. So, the strain induced transformation will enhance ductility if retained

austenite is moderately stable against straining. It is well established that the strain induced transformation of austenite to martensite takes place between the M_S temperature (martensite start temperature), and the M_d temperature, above which the austenite becomes completely stable [46,47]. Therefore, there is a temperature between M_S and M_d at which the strain induced transformation is suppressed moderately and the resultant strain hardenability is held in a large strain range, leading to maximum benefit of the TRIP effect.

Characterisation of the deformed microstructure.

In an attempt to depict the role of austenite in the ductility behavior of these microstructures, different cuts of the tested tensile samples were prepared according to scheme in Figure 6, where the grey areas represent the position where the cuts were intended and the black area represents the selected area for observation and analysis. T4 represents the un-deformed region and FS the fracture surface, being T1 just few mm beneath the FS. Hardness in Figure 7 a clearly indicates a hardening of the microstructure as the level of deformation increases form T4 towards T1, consequence of the strain hardening and the formation of high C martensite by TRIP effect.

The evolution of the fraction of austenite at the different positions in Figure 6, is presented against the estimated reduction in area, Figure 7 b, after measuring the diameter of the disks cut at different positions, and some important information can be extracted. At the fracture surface (FS) no evidence of austenite has been found, but just beneath it, zone T1, is possible to observe that not all the austenite has transformed to martensite, almost 15% of retained austenite remains untransformed in both cases. Even though, transformation of this 15% of austenite hardly represents any benefit in ductility, as expected when TRIP effect is taking place close to the fracture state of the test. The noticeable difference is that for the 200ºC microstructure T1 represents≈ 7% of area reduction while for the 250ºC is ≈32%. It is also evident that about 20% of retained austenite transforms, up to T1 zone, and still the ductility achieved in one and the other microstructure is very different, as it is the rate of austenite transformation, Figure 7 b. Another interesting fact is that the remaining un-transformed austenite, up to T1 zone, remains within the

limits of what is considered the percolation threshold. It has been suggested that with microstructures of the kind considered here, failure in a tensile test occurs when the retained austenite loses continuity [48,49] and that this percolation threshold is reached when the austenite fraction is about 10%, grey shadowed area in Figure 7 b where is has been considered a 3% of error. Or in other words, it seems that the formation of hard, strain induced martensite can only be tolerated if the austenite maintains a continuous path through the test sample.

When C in retained austenite from both treatments is compared, Table 2, it is clear that stability of austenite in the microstructure at 250ºC must be higher than that at 200ºC, 1.47 v.s 1.22 wt.%, also evident at the rate at which transforms to martensite, higher in the 200ºC than in the 250ºC microstructure, see Figure 7 b. A wide distribution of retained austenite sizes in the microstructure lead to effective variations of the austenite stability, being favorable for spreading the effect of the transformation all along straining and for postponing localization [50,51]. As it has been mentioned, and recently probed at an atomic level for these type of alloys [24,32], there is a strong correlation between the size of the austenite feature and the amount of C that keeps in solution, the smaller the higher the amount of C is. Therefore attending to results in Figure 4, it can be concluded that a wider distribution of austenite sizes, wider range of levels of mechanical stabilities, might be an extra contribution to ductility. In this sense, a detailed observation of the X-ray peaks profile at the different deformation stages, Figure 7 c, also reveals that austenite lattice parameter tends to increase as deformation increases, which is linked with the fact that austenite with lower C content transform first to martensite, mechanically less stable [46] being the remaining austenite richer in C, therefore having a bigger lattice parameter. The intensity of the austenite peaks also decreases as deformation increases, i.e. austenite transforms to martensite. The transformation from austenite to martensite as deformation increases, TRIP effect, leads to asymmetry and shifting of the ferrite peaks, because martensite and ferrite share the same 2θ positions.

Finally the strength mismatch between the different phases (bainite and austenite) may play an important factor controlling the stability of retained austenite [50,52,53]. Medium strength ratio of 2nd phase (austenite) /matrix (ferrite) avoids or retard stress concentrations, i.e. in the case of the microstructure obtained at 200ºC, a slightly harder matrix, as ferrite contains more C, and a lower C content of austenite,

mechanically weaker, makes the YS_γ / YS_α ratio lower in this case than in the 250ºC. In other words, the matrix might be playing an important role in the stability and efficiency of TRIP effect.

4 CONCLUSIONS

It has been possible to design a low temperature bainitic steel with the same mechanical properties, microstructure and transformation kinetics, as the best alloys up to date, but without the expensive use of Co and Al and lower Cr and Mn contents. The design is merely based on the use of Si as an austenite strengthener, from where the incredibly fine and slender plates of bainitic ferrite will grow. The bainitic microstructure was obtained at two isothermal temperatures, 220 and 250ºC.

In spite of the widely accepted limit of 1.5% to suppress cementite formation, it has been shown that this extra addition allows to retain significant quantities of retained austenite at the end of the bainite reaction. The resulting microstructure has exhibited unprecedented ductility during tensile tests, with uniform elongation above 10% for a UTS above 2 GPa. After a full characterization of the microstructures and their tensile properties, it could only be concluded that the composite character of the microstructure formed by two phases (bainitic ferrite and austenite) with a complex, interconnected structure, activates several mechanisms that contributes to the strength and ductility of this novel microstructure.

5 ACKNOWLEDGEMENTS

The authors gratefully acknowledge the support of the European Research Fund for Coal and Steel and the Spanish Ministry of Science and Innovation Plan Nacional de I+D+I (2008-2011) for funding this research under the contracts RFSR-CT-2008-00022, and MAT2010 - 15330 respectively. J. Cornide also acknowledges the Spanish Ministry of Science and Innovation for financial support in the form of a PhD research grant (FPI).

6 REFERENCES

1. T. Yokota, C. Garcia-Mateo, H.K.D.H. Bhadeshia, Scri. Mater., 51 (2004) 767-770.
2. F.G. Caballero, H.K.D.H. Bhadeshia, K.J.A. Mawella, D.G. Jones, P. Brown, Mater. Sci. Technol., 18 (2002) 279-284.
3. C. Garcia-Mateo, F. G Caballero, H.K.D.H. Bhadeshia. ISIJ Int., 43 (2003) 1238-1243.
4. C. Garcia-Mateo, F. G Caballero, H.K.D.H. Bhadeshia. ISIJ Int., 43 (2003) 1821-1825
5. F.G. Caballero, H.K.D.H. Bhadeshia, Curr. Opin. Solid State Mater. Sci., 8 (2004) 251-257.
6. J. Yang, T.S. Wang, B. Zhang, F.C. Zhang, Mater. Des., 35 (2012) 170-174.
7. M.N. Yoozbashi, S. Yazdani, T.S. Wang, Mater. Des., 32 (2011) 3248-3253.
8. J.A.D.C. Junior, I.P. Pinheiro, T.F.M. Rodrigues, V.D.C. Viana, D.B. Santos, in: 18th IFHTSE Congress - International Federation for Heat Treatment and Surface Engineering, Rio Janeiro, 2010, pp. 4683-4691.
9. H.K.D.H. Bhadeshia, Proc. R. Soc. A, 466 (2010) 3-18.
10. I.B. Timokhina, H. Beladi, X.Y. Xiong, Y. Adachi, P.D. Hodgson, Acta. Mater., 59 (2011) 5511-5522.
11. S.B. Singh, H.K.D.H. Bhadeshia. Mater. Sci.. Eng A. 245 (1998) 72-79
12. C.H. Young, H.K.D.H. Bhadeshia. Mater. Sci. Technol. 10 (1994) 209-214.
13. M. Peet. “Modelling the Hot-Deformation of Austenite” Master of Philosophy Thesis. University of Cambridge, 2001.
14. F.G. Caballero, H. Roelofs, St. Hasler, C. Capdevila, J. Chao, J. Cornide, C. Garcia-Mateo. Mater. Sci. Technol. 28 (2012) 95-102.
15. H.K.D.H. Bhadeshia. Bainite in Steels. 2nd Edition. 2001 by The IOM of London. 1 Carlton House Terrace, London.
16. F. G. Caballero, M. J. Santofimia, C. Capdevila, C. García-Mateo, C. García de Andrés. ISIJ Int. 46 (2006) 1479-1488.
17. C. Garcia-Mateo, F.G. Caballero. Int. J. Mater. Res. 98 (2007) 137-143.

18. F.G. Caballero, M.K. Miller, C. Garcia-Mateo, C. Capdevila,C. Garcia de Andrés. JOM. 60 (2008) 16-21.
19. L.C. Chang, H. Bhadeshia, Mater. Sci. Technol., 11 (1995) 874-881.
20. J. Dyson, B. Holmes. J. Iron Steel Inst. 208 (1970) 469-474.
21. C. Garcia-Mateo, M. Peet, F.G. Caballero, H.K.D.H. Bhadeshia. Mater. Sci. Technol. 20 (2004) 814-818.
22. F.G. Caballero, M.K. Miller, S.S. Babu, C. Garcia-Mateo, Acta Mater., 55 (2007) 381-390.
23. C. Garcia-Mateo, F.G. Caballero. Mater. Trans. JIM. 46 (2005) 1839-1846.
24. C. Garcia-Mateo, F.G. Caballero, M.K. Miller, J.A. Jimenez. J. Mater. Sci. 47 (2012) 1004-1010.
25. H.K.D.H.Bhadeshia, D.V. Edmonds. Metall. Trans., 10 (1979) 895-907.
26. L.C. Chang, H.K.D.H. Bhadeshia. Mater. Sci. Technol., 11 (1995) 105-108.
27. F.G. Caballero, H-W. Yen, M.K. Miller, J-R Yang, J. Cornide, C. Garcia-Mateo. Acta Mater., 59 (2011) 6117-6123.
28. F.G. Caballero, M.J. Santofimia, C. García-Mateo, J. Chao, C.G. de Andrés, Mater. Des., 30 (2009) 2077-2083.
29. F.G. Caballero, M.K. Miller, C. Garcia-Mateo, Acta Mater., 58 (2010) 2338-2343.
30. H.K.D.H. Bhadeshia, A.R. Waugh, Acta Metall., 30 (1982) 775-784.
31. A.J. Clarke, J.G. Speer, M.K. Miller, R.E. Hackenberg, D.V. Edmonds, D.K. Matlock, F.C. Rizzo, K.D. Clarke, E. De Moor, Acta. Mater., 56 (2008) 16-22.
32. F.G. Caballero, M.K. Miller, A.J. Clarke and C. Garcia-Mateo. Scr. Mater., 63 (2010) 442-445.
33. C. Garcia-Mateo, F.G. Caballero, ISIJ Int., 45 (2005) 1736-1740.
34. C. Herrera, D. Ponge, D. Raabe. Acta Mater., 59 (2011) 4653-4664.
35. S. Curtze, V.T. Kuokkala. Acta Mater., 58 (2010) 5129-5141.
36. A. Dumay, J.-P. Chateau , S. Allain , S. Migot , O. Bouaziz. Mater. Sci. Eng. A, 483-484 (2008) 184-187.

37. Lin Li, T. Y. Hsu(Xu Zuyao). Calphad., 21 (1997) 443-448.
38. S. Allain , J.-P. Chateau , O. Bouaziz , S. Migot , N. Guelton , Mater. Sci. Eng. A 387-389 (2004) 158-162.
39. MTDATA: Phase Diagram Software from the National Physical Laboratory, Teddington, UK (2004)
40. B. P. J. Sandvik, H. P. Nevalainen, Met. Technol. 15 (1981), 213-220.
41. H. K. D. H. Bhadeshia, D. V. Edmonds. Met. Sci. 17 (1983) 411-419.
42. C. A. N. Lanzillotto, F. B. Pickering. Met. Sci. 16 (1982) 371-382.
43. N. K. Balliger, T. Gladman. Met. Sci. 15 (1981) 95-108.
44. P.J. Jacques, E. Girault , A. Mertens , B. Verlinden, F. Delanny. ISIJ Int. 41 (2001) 1068-1074.
45. K. Nohara, Y. Ono and N. Ohashi. J. Iron Steel Inst. Jpn. 63 (1977) 212-222.
46. M. Sherif, C. Garcia-Mateo, T. Sourmail, H.K.D.H Bhadeshia. Mater. Sci. Technol. 20 (2004) 319-322.
47. F.G. Caballero, C. Garcia-Mateo, J. Chao, M.J. Santofimia, C. Capdevila, C Garcia de Andres. ISIJ Int. 48 (2008) 1256-1262.
48. H. K. D. H. Bhadeshia: Ironmak. Steelmak. 34 (2007) 194-199.
49. M. Sherif. “Characterisation and development of nanostructured, ultrahigh strength, and ductile bainitic steels”.PhD Thesis. University of Cambridge, 2005.
50. F. Lani , Q. Furnemont , T. Van Rompaey , F. Delannay , P.J. Jacques, T. Pardoen. Acta Mater., 55 (2007) 3695-3705.
51. K. Hase, C. Garcia-Mateo, H.K.D.H. Bhadeshia. Mater. Sci. Eng. A, 438-440 (2006) 145-148.
52. J. H. Ryu, Dong-Ik Kim, H. S. Kim, H.K.D.H. Bhadeshia. Dong-Woo Suh. Scr. Mater. 63 (2010) 297-299.
53. T. Hojo, K.I. Sugimoto, Y. Mukai, S. Ikeda. ISIJ Int. 48 (2008) 824-829.

Table 1. Chemical composition, all in wt.%.

	C	Si	Mn	Cr	Cu	Ni	P	S
1CSi	0.98	2.90	0.77	0.45	0.21	0.16	0.016	0.014

Table 2. Quantitative data on microstructure. V_i and C_i stands for the fraction and C content of the phase i, where i could be, α_b = bainitic ferrite and γ = austenite. t stands for the plate thickness of bainitic ferrite, γ_{film} and γ_{block} stands for the thickness of both morphologies of retained austenite size, a_γ is the austenite lattice parameter.

Samples	a_γ/nm	$V_{\alpha b}$	V_γ	$C_{\alpha b}$/wt.%	C_γ/wt.%	t/ nm	γ_{film}/nm	γ_{block}/nm
220ºC	0.362	0.64±0.02	0.36±0.01	0.08±0.06	1.22±0.06	28±2	34±1	630±19
250ºC	0.363	0.66±0.02	0.34±0.01	0.05±0.06	1.47±0.06	28±1	37±2	870±29

Table 3. Summary of mechanical properties. U = uniform, F= fracture, Elon. = Elongation. HV_{10} = Hardness Vickers 10kg

	YS/ MPa	UTS/MPa	U. Elon./%	F. Elon./%	HV_{10}
1CSi-220ºC	1704±21	2287±19	7.4±1.7	7.4±1.7	664±9
1CSi-250ºC	1698±33	2068±8	11.6±0.5	21.3±0.9	613±20

Table 4. SFE calculated for retained austenite in 220 and 250ºC microstructures and for a TWIP steel from ref.32, *where the estimated value of the SFE of the TWIP steel is aprox. 0.044 mJ m-2.

	SFE mJ m^{-2}
	($x10^3$)
TWIP	0.046*
250ºC	0.82
220ºC	1.06

Figures Captions

Figure 1. Examples at different magnifications of the microstructures obtained by isothermal transformation at, 220ºC (a) and (c) and 250ºC and (b) and (d).

Figure 2. TEM micrograph detailing dislocation debris the microstructure obtained at 250ºC.

Figure 3. Bainitic ferrite plate thickness distribution and average value.

Figure 4. Retained austenite morphologies distribution and average size.

Figure 5. Typical stress-strain curves and incremental strain-hardening exponent n evolution with true strain.

Figure 6. Scheme of the cuts performed on tested tensile specimens. Grey areas represent the position where the cut was intended and the black area represents the selected area for observation and analysis.

Figure 7. Summary of (a) HV10, (b) retained austenite evolution with the degree of deformation, measured as the reduction of area after measuring the diameter of the disks cut at different positions and (c) X-ray peak profile of the 250ºC microstructure at different stages of deformation.

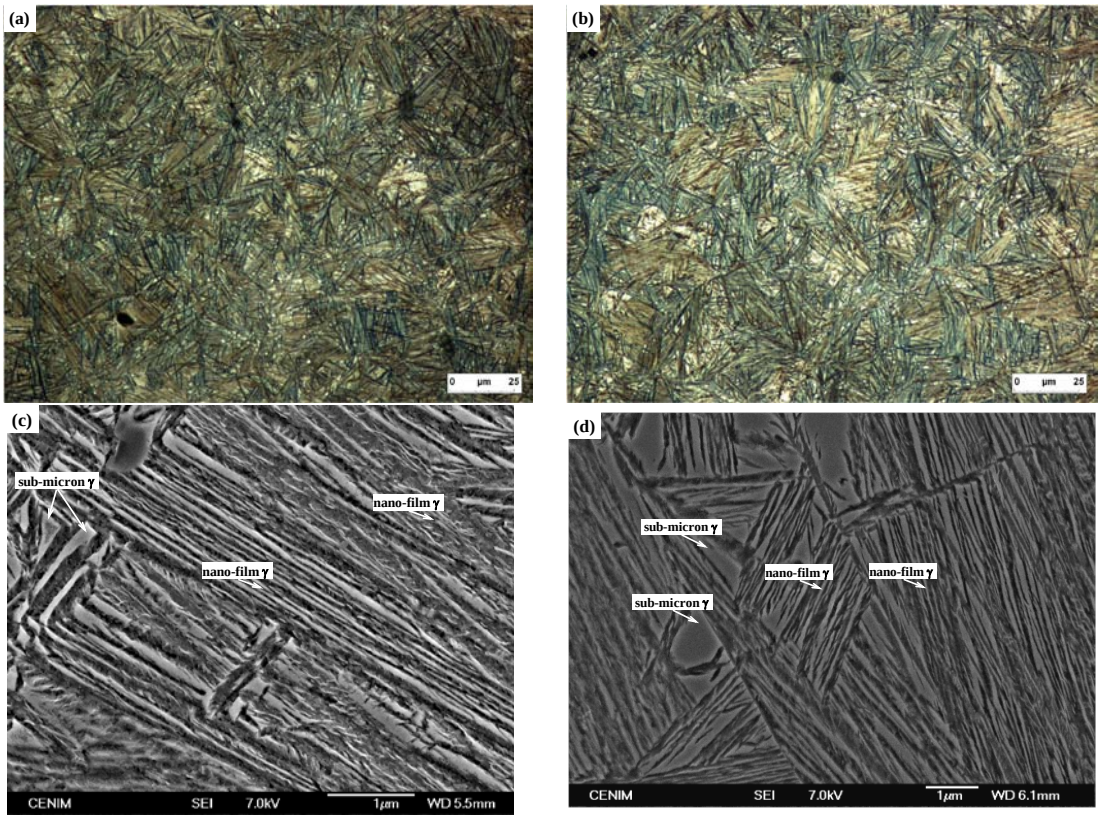

Figure 1. Examples at different magnifications of the microstructures obtained by isothermal transformation at, 2200ºC (a) and (c) and 250ºC and (b) and (d).

Figure 2. TEM micrograph detailing dislocation debris the microstructure obtained at 250ºC.

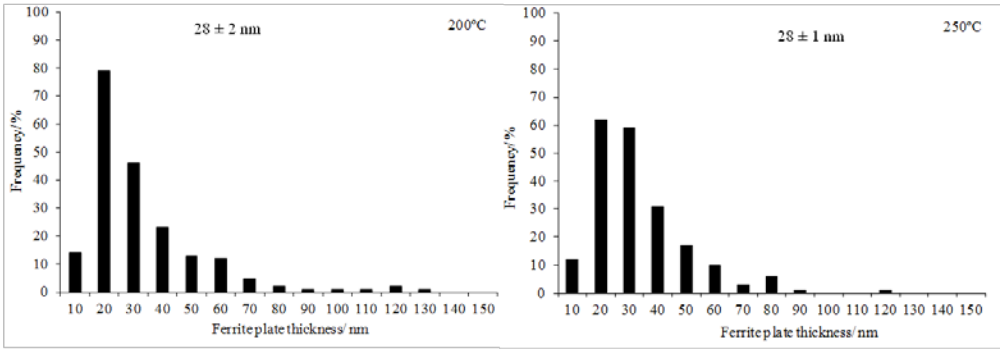

Figure 3. Bainitic ferrite plate thickness distribution and average value.

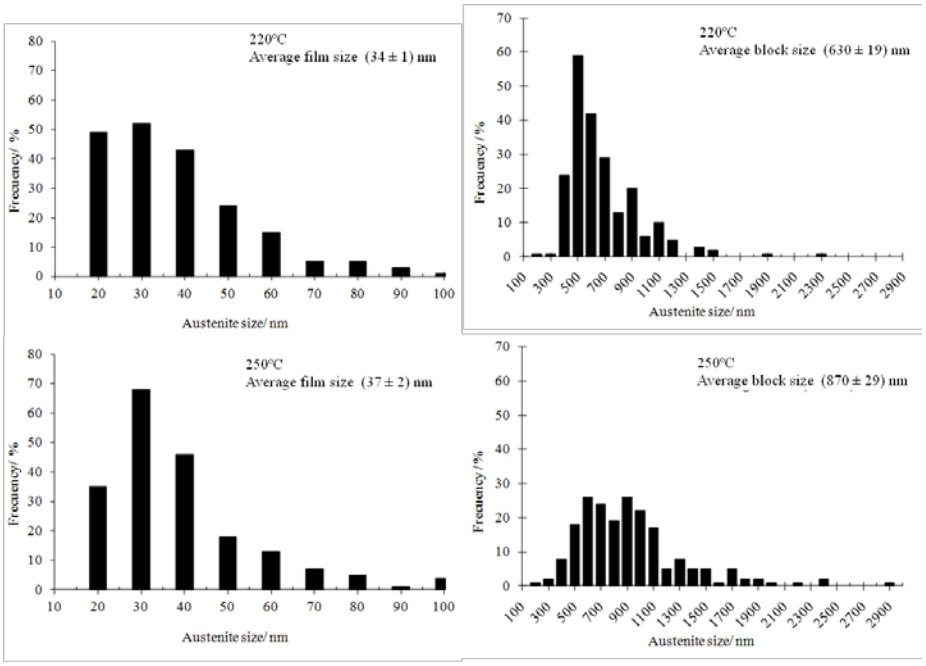

Figure 4. Retained austenite morphologies distribution and average size.

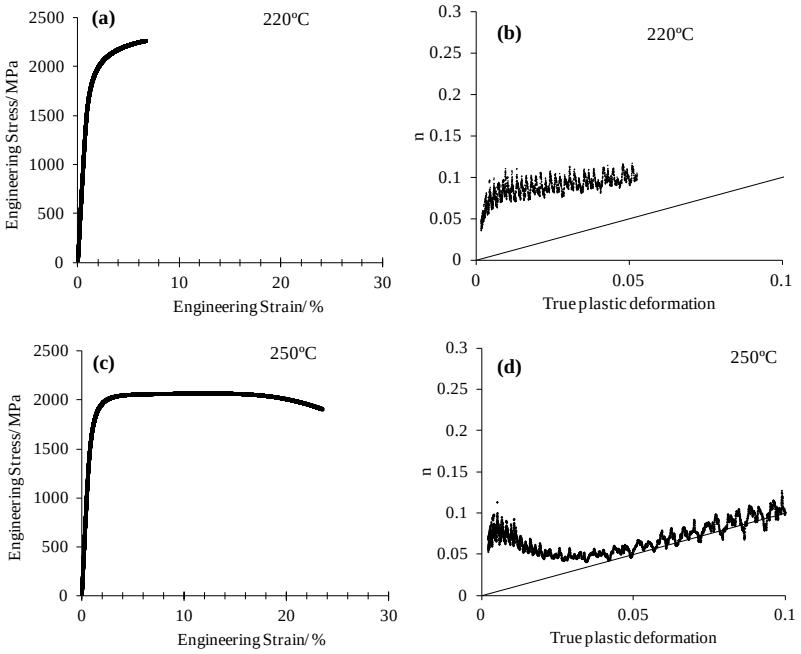

Figure 5. Typical stress-strain curves and incremental strain-hardening exponent n evolution with true strain.

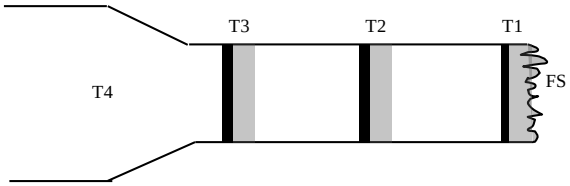

Figure 6. Scheme of the cuts performed on tested tensile specimens. Grey areas represent the position where the cut was intended and the black area represents the selected area for observation and analysis.

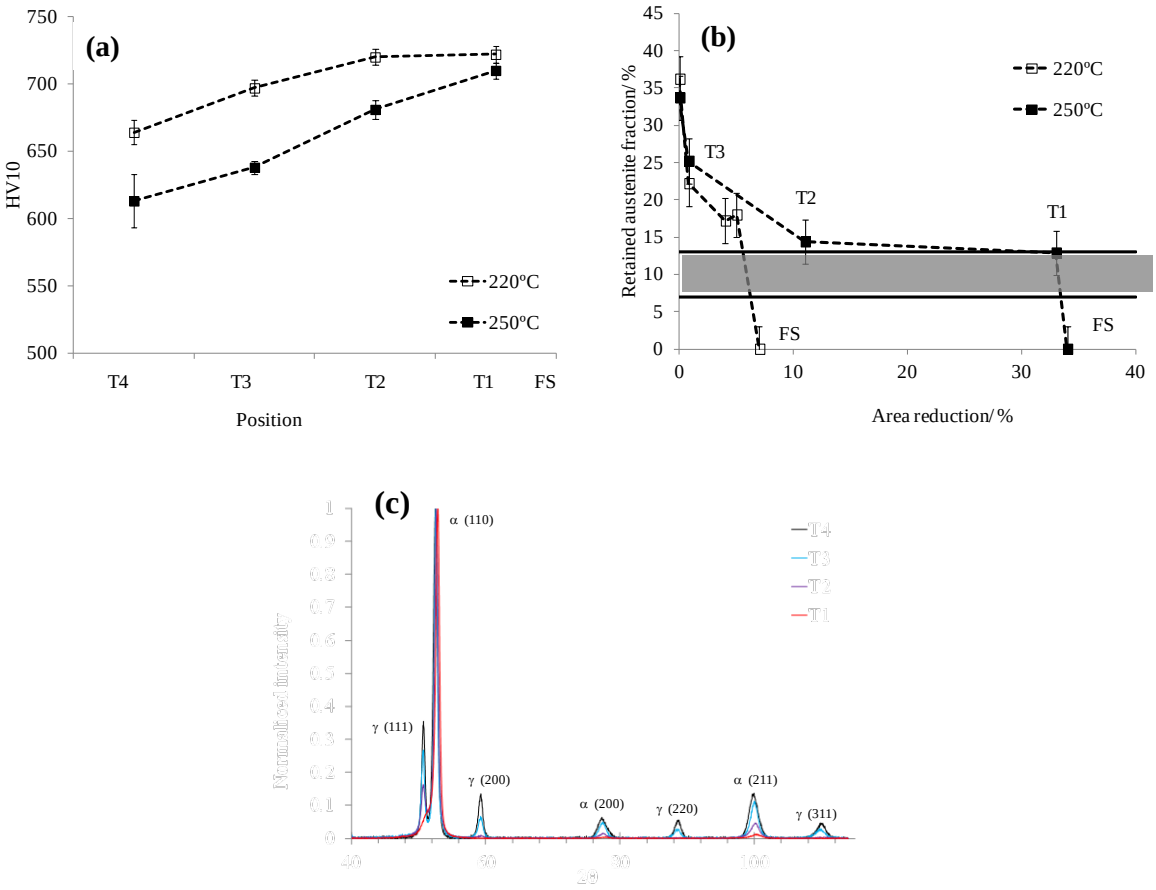

Figure 7. Summary of (a) HV10, (b) retained austenite evolution with the degree of deformation, measured as the reduction of area after measuring the diameter of the disks cut at different positions and (c) X-ray peak profile of the 250ºC microstructure at different stages of deformation.